EPJ E
Soft Matter and Biological Physics
EPJ.org
your physics journal

Eur. Phys. J. E (2013) **36**: 134 DOI 10.1140/epje/i2013-13134-8

Order and frustration in liquid-crystalline dendrimers

B.I. Ostrovskii, S.N. Sulyanov, N.A. Boiko, V.P. Shibaev, S.B. Astaf'ev, L.G. Yanusova and W.H. de Jeu

edp sciences Società Italiana di Fisica Springer

Eur. Phys. J. E (2013) **36**: 134
DOI 10.1140/epje/i2013-13134-8

THE EUROPEAN PHYSICAL JOURNAL E

Regular Article

Order and frustration in liquid-crystalline dendrimers

B.I. Ostrovskii[1,a], S.N. Sulyanov[1], N.A. Boiko[2], V.P. Shibaev[2], S.B. Astaf'ev[1], L.G. Yanusova[1], and W.H. de Jeu[3]

[1] Institute of Crystallography Academy of Sciences of Russia, Leninsky pr. 59, 119333 Moscow, Russia
[2] Department of Chemistry, Moscow State University, 1 Leninskie Gory, 119992 Moscow, Russia
[3] DWI at RWTH-Aachen University, D-52056 Aachen, Germany

Received 7 August 2013 and Received in final form 23 October 2013
Published online: 28 November 2013 –

Abstract. X-ray diffraction has been used to elucidate the structure and phase behavior of several liquid-crystalline dendrimers with a different surface topology of the terminal chains. This includes second-generation liquid-crystalline block and statistical dendrimers with mixed aliphatic and mesogenic terminal groups as well as homo-dendrimers of several generations containing only mesogenic end groups. The homo-dendrimers of generation one to four display a monolayer smectic phase, while the fifth generation shows a more ordered columnar phase. The block-dendrimer of the second generation has a bilayer smectic phase. The precise structure of the lamellar ordering has been determined by X-ray reflectivity from thin films on a substrate. The second-generation statistical dendrimer does not show any mesogenic phase. The observed phase behavior is discussed in terms of the frustration due to competition between the stiff geometry of the dendritic matrix and the close-packing conditions of the terminal chains.

1 Introduction

Frustration effects are implicit in many physical systems as different as spin glass magnets, adsorbed monomolecular films and liquid crystals [1–3]. The common feature of such systems is the presence of two or more competing interactions favoring different periodicities. In liquid crystals (LC) frustration effects are well known for molecules with strongly polar terminal groups —so-called dipolar frustrations. In these materials a variety of smectic phases with a layer spacing incommensurate with the length of a single molecule has been observed as well as re-entrant phenomena [4–7]. In the latter case, the smectic layer structure is destroyed and the less ordered nematic phase re-appears upon cooling or increasing pressure. Alternatively, frustration might be relieved either by the appearance of a periodic array of defects [6,8], or by the formation of a phase with two-dimensional (2D) periodicity, of a type of columnar phase [1,5,9,10]. Similar effects have also been reported for sterically strongly asymmetric mesogens [11–13] and for polyphilic LCs containing chemically distinct molecular fragments [14–16]. In this context LC dendrimers represent *intrinsically* frustrated systems due to their complex topological and chemical structure. First, the relatively stiff spherical dendrimer cores favor a close-packed 3D packing, while the mesogenic terminal chains tend to form uniaxial phases like nematic or smectic. Second, terminal chains of various natures (aromatic and aliphatic) in the same dendrimer molecule potentially lead to segregation, thereby increasing possible types of order. The aim of the present work is to study the effect of the molecular architecture of LC dendrimers on their phase stability and structure for various combinations of terminal fragments.

LC dendrimers occupy a niche at the intersection of liquid crystals and polymers. In the ideal case, dendrimers can be described as monodisperse macromolecules with a regular and highly branched 3D structure [17–19]. During the last two decades a number of molecular designs have been produced that combine a dendritic structure with liquid crystallinity [20–23]. More recently the family of LC dendrimers was enriched by dendrimer molecules with terminal bent-core fragments [24] and by "Janus" dendrimers, formed by the segmented structures containing two different types of mesogenic units [25–28]. Carbosilane LC dendrimers are of particular interest because of their thermodynamic stability and wide range of molecular architectures due to the specific chemical properties of silicon [29,30]. Mesogenic groups can be covalently linked to the dendrimer's periphery by flexible aliphatic chains, effectively decoupling the mesogenic moiety from the relatively stiff dendritic core [31–34]. Naively one would expect the branched topology of dendrimers to lead to spherical symmetry. This would contradict the formation of LC phases, which require anisotropy in molecular shape and as well as in molecular interactions. However, dendrimers with terminal mesogenic groups show, in dependence of their generation number n and the chemical nature of

[a] e-mail: ostrenator@gmail.com

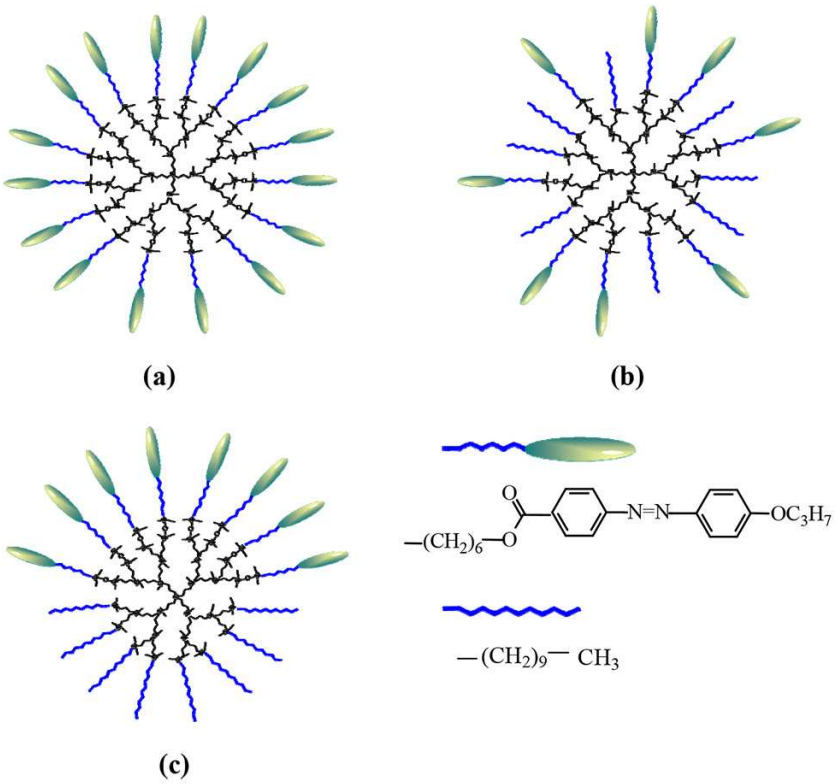

Fig. 1. Schematic representation of the structure of the carbosilane LC dendrimers of second generation containing two types of terminal chains: mesogenic azobenzene (ellipsoid) and aliphatic decyl chain (zig-zag). (a) G-2-homo, (b) G-2-stat and (c) G-2-block. The sketches show the isotropic dendrimer conformations with the mesogenic (aliphatic) groups distributed uniformly on the periphery. On condensation into a mesomorphic state the dendrimer will, on average, become prolate or oblate.

the terminal mesogenic fragments, both lamellar (smectic) mesophases and various types of columnar mesophase [30]. Here n is determined by the number of the sequential branching of the dendritic core of the molecule. X-ray investigations indicate for low generation (n = 1–3) only lamellar phases, while higher generations (n = 4–5) can form both lamellar and columnar mesophases [35–38].

The different structures formed by LC dendrimers imply that the overall shape of the molecules can change. Evidently, there is sufficient conformational freedom to rearrange the distribution of the terminal mesogenic groups to form various LC phases. However, the underlying mechanisms are currently not well understood. Also hardly data are available on structure and phase behavior of LC dendrimers with different type of terminal chains (like aromatic and aliphatic). In this work we have used X-ray techniques to study carbosilane homo-, block-, and statistical dendrimers with a different surface topology (see fig. 1). First we discuss various generations of LC homo-dendrimers with a terminal mesogenic azobenzene group. In agreement with the known general trend, generation one to four form a monolayer smectic phase, while the fifth generation shows a columnar phase. Next a second-generation (G-2) dendrimer is considered in which from the sixteen terminal mesogenic groups eight are replaced by long aliphatic chains. In the G-2 block-dendrimer two corners of the silicon tetrahedral matrix connect mesogenic groups, while the two others possess only aliphatic chains. In the statistical G-2 dendrimer this occupation is arbitrary (see fig. 1). In the latter case two different crystalline phases and a direct transition to the isotropic phase are observed. For the G-2 block-dendrimer segregation occurs between chemically distinct aromatic and aliphatic moieties. In addition a bilayer smectic phase is found with a spacing about twice of the corresponding homo-dendrimer.

2 Experimental

The G-n-homo (n = 2–5) and G-2-stat carbosilane dendrimers were synthesized by hydrosilylation of carbosilane dendritic matrices containing terminal allyl groups with either a mesogene containing fragment (G-n-homo) or a mixture of mesogens and aliphatic fragments (G-2-stat) [31,37]. The structures were proven by ^{1}H NMR spectroscopy while the purity was checked by GPC, providing also a value of polydispersity index $M_w/M_n = 1.03$. The carbosilane block dendrimer was synthesized using a special half-protection technique [39,40].

The phase sequences of the LC dendrimers were determined by DSC, optical polarization microscopy and X-ray diffraction. Upon heating the G-2-homo and G-2-block dendrimers, the low temperature crystalline phase

Table 1. Phase behaviour of the LC dendrimers investigated. Cr stands for crystalline phase, SmA for smectic-A phase, Col_{rec} for rectangular columnar phase, G for glassy state and I for isotropic liquid.

LC Dendrimer	Phase transitions (°C)
G-2-homo	Cr 8.0 SmA 62.0 I
G-2-block	Cr 12.0 SmA 40.0 I
G-2-stat	Cr_1 −16.5 Cr_2 1.5 I
G-3-homo	Cr 3.0 SmA 58.0 I
G-4-homo	Cr 3.0 SmA 59.0 I
G-5-homo	G −22.0 Col_{rec} 62.0 I

is replaced by the lamellar SmA phase. The G-2-stat dendrimer shows no mesophases; instead two crystalline phases are observed with a direct transition to the isotropic phase. The phases and their transition temperatures are given in table 1 and depend on the composition and the distribution of the terminal groups on the surface of the dendritic matrix. The G-*n*-homo dendrimers of generation two to four display a SmA phase intermediate between crystalline and isotropic phases. For the fifth generation this lamellar phase is replaced by a columnar one.

Bulk X-ray data were taken at the "Belok" beam line in the Kurchatov Synchrotron Centre (Moscow, Russia) using monochromatic radiation ($\lambda = 0.0985\,\mathrm{nm}$) [41] at a sample-to-detector distance of 0.28 m. Defining the wave vector transfer $q = (4\pi/\lambda)\sin\theta$, where 2θ is the scattering angle, the resolution in the scattering plane was about $\Delta q \approx 0.08\,\mathrm{nm}^{-1}$ (full width at half maximum, FWHM). The LC dendrimers were placed in a circular opening (diameter about 2 mm) in a stainless steel plate. Powder-like 2D X-ray scattering patterns were recorded with a Mar CCD detector (Rayonix SX165, 2048×2048 pixels). Cross-sections $I(q)$ were determined by averaging over narrow rectangular regions [42,43]. The measurements were performed at room temperature. The G-2-stat sample was additionally investigated at temperatures below 0 °C in order to determine the range of stability of the different phases.

Additional X-ray reflectivity (XRR) measurements were performed on the G-2-block dendrimer at the FOM-Institute AMOLF (Amsterdam) using a triple-axis diffractometer and Cu$K\alpha$ radiation ($\lambda = 0.154\,\mathrm{nm}$) from a rotating anode X-ray generator (Rigaku RU-300H, 18 kW). By employing a parabolic multilayer mirror (Bruker, Karlsruhe), a highly parallel beam was obtained (divergence about 20 mdeg). For XRR measurements the films with a thickness ranging from 50 to 120 nm were prepared by spin-coating from toluene solutions onto a float silicone/glass substrate. The films were annealed for about 30 hours in the SmA phase at room temperature in a dry nitrogen atmosphere. In reciprocal space, the specularly scattered intensity is a function of q_z with the z-axis perpendicular to the film. The reflected intensity $I(q_z)$ has been calculated using the recursive matrix solution of the Fresnel equations for the reflectivity of a multilayer system derived by Parrat [44] and was convoluted with the experimental resolution of $\Delta q_z = 0.04\,\mathrm{nm}^{-1}$. The reflectivity simulations and fitting were processed using the software package BARD [45,46]. The films were modeled by a succession of parallel homogeneous slabs, each of them characterized by three parameters: thickness, electron density and interfacial roughness described by Gaussian statistics.

Table 2. Variation of the smectic layer spacing for G-*n*-homo dendrimers.

LC Dendrimer	d (nm)
G-1-homo	3.79 [(a)]
G-2-homo	4.15
G-3-homo	4.48
G-4-homo	4.66

[(a)] Data provided by R.M. Richardson, Bristol, UK.

3 Results

3.1 G-n-homo dendrimers

X-ray diffraction in the low-angle region of the G-2-homo dendrimer reveals equally spaced layer reflections as expected for a smectic phase, fig. 2a. The corresponding periodicity is $d \approx 4.15\,\mathrm{nm}$. The diffraction peaks are resolution-limited, indicating that the coherently scattered size in the sample along the layer normal is at least $L = 2\pi/\Delta q \approx 80\,\mathrm{nm}$ or about 20 smectic layers. Broad in-plane scattering occurring at larger angles corresponds to distances of about 0.4–0.6 nm. The diffuse profile can be well fitted by superposition of two Lorentzians centered at $q_1 \approx 11.02\,\mathrm{nm}^{-1}$ ($d_1 = 0.57\,\mathrm{nm}$) and $q_2 \approx 14.27\,\mathrm{nm}^{-1}$ ($d_2 = 0.44\,\mathrm{nm}$), fig. 2b. The presence of two characteristic lengths is quite common for polyphilic mesogens [15]. The first dimension of $d \approx 0.57\,\mathrm{nm}$ relates to the liquid structure of the carbosilane fragments within the dendrimer matrix, while the second one, $d \approx 0.44\,\mathrm{nm}$, corresponds to correlations of the flexible alkyl chains. The short-range in-plane order is characterized by correlation lengths $\xi_1 \approx \xi_2 = 2/\Delta q = 0.7$–$0.9\,\mathrm{nm}$, a few molecular diameters, quite normal for liquid order.

The packing of the LC dendrimer molecules along the layer normal is pictured schematically in fig. 3. To fit the experimental layer period $d = 4.15\,\mathrm{nm}$, the mesogenic azobenzene moieties of neighboring layers should fully overlap. Furthermore, the molten hydrocarbon spacer groups provide the necessary conformational freedom to accommodate the cylinder-like molecular shape that favors a lamellar phase. The resulting layer configuration identifies close packing of overlapping mesogenic units as responsible for the formation of the smectic mesophase.

The G-*n*-homo dendrimers for $n = 3, 4$ behave similarly as for $n = 2$. Their layer periods are presented in table 2. The results indicate a systematic increase of ~ 0.2 to 0.3 nm per generation, consistent with the increased

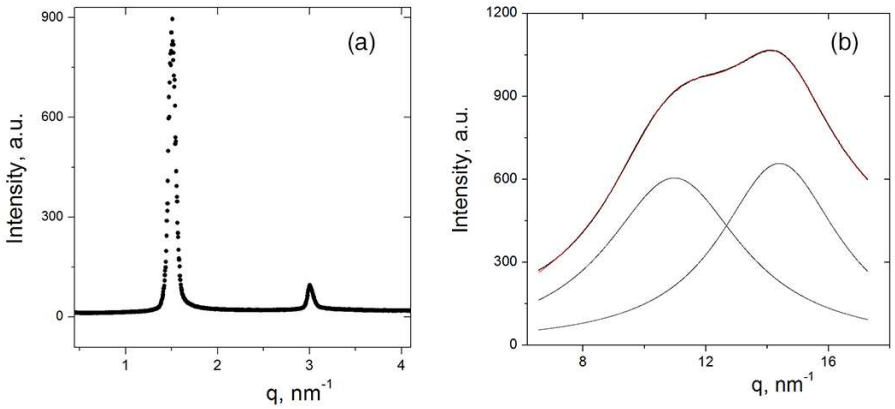

Fig. 2. X-ray diffraction profiles of the G-2-homo dendrimer in the SmA phase. (a) Small-angle area. (b) Wide-angle diffuse peaks. The solid line fitted to the data points is the sum of Lorentzian peaks shown below.

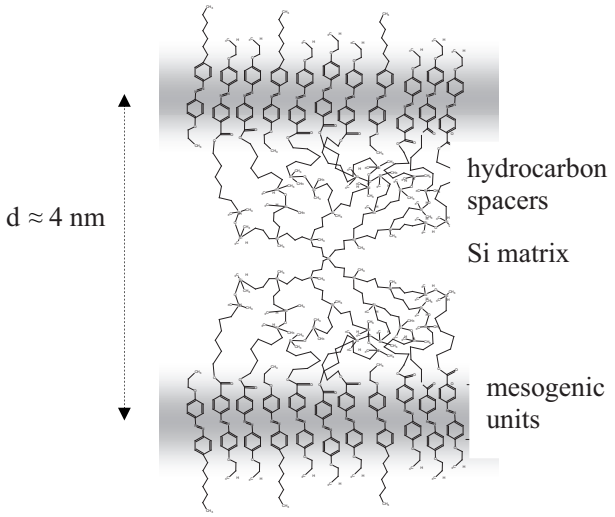

Fig. 3. Cross-section of the single-layer smectic ordering of the G-2-homo dendrimer. The region of overlapping terminal mesogens is highlighted by shades of gray.

size of the dendritic core. The short-range in-plane order is characterized by the same two lengths scales, 0.57 and 0.44 nm, found earlier for G-2-homo.

The X-ray peaks of the G-5-homo dendrimer show a very different low-angle diffraction pattern, fig. 4a, with no harmonic relation. In the wide-angle region a double peaked diffuse profile is observed similar as for the lower generation homo-dendrimers, fig. 4b. These results indicate a columnar phase, characterized by a 2D in-plane lattice and liquid-like order in the perpendicular direction. Though the highly symmetrical shape of LC dendritic molecules would suggest a hexagonal in-plane structure, this is not compatible with the observed sequence of peaks, fig. 4a. Alternatively, we assume 2D rectangular cell characterized by unit-cell parameters a and b. This could be either primitive with one molecule per elementary unit, or centered rectangular ($C2mm$ symmetry) with an additional molecule in the cell center, fig. 5. All three types

Table 3. X-ray results for the columnar rectangular phase ($\mathrm{Col_{rec}}$) of the G-5-homo dendrimer.

q_{exp} (nm^{-1})	d_{exp} (nm)	d_{calc} (nm)	Indexing (hk)
1.18	5.322	5.32	02
1.55	4.058	4.06	11
2.28	2.752	2.75	13
2.83	2.224	2.22	20
3.11	2.019	2.02	22

of columnar phases (simple rectangular, centered rectangular and hexagonal) are known to exist among LC dendrimers [37,38]. For centered rectangular cell corresponding to the plane group $C2mm$ extinction rules indicate that only reflections with Miller indices satisfying $h+k=$ even integer should be present. From table 3 we see that this is indeed the case. Thus for the G-5-homo dendrimer we deal with a centered 2D lattice with the unit-cell parameters $a = 4.39$ nm and $b = 10.64$ nm. Perpendicular to the lattice plane the dendrimer molecules form columns that are internally disordered: $\mathrm{Col_{rec}}$ mesophase. Based on dense packing we assume elliptical molecular cross-sections in the ab-plane as pictured in fig. 5.

Elliptically shaped molecules can aternatively be packed in the nodes of a 2D rectangular lattice with $P2gg$ symmetry. For this type of centered lattice the orientation of the ellipses alternates (herringbone like). Extinction conditions require that h, respectively k, must be even for reflections $(h0)$ and $(0k)$. However, $h+k$ can be both even and odd for $h,k \neq 0$, [47]. Accordingly, the lowest-order reflections allowed for $P2gg$ are (12) and (21). In fig. 4a these are absent, making our assignment as $C2mm$ more plausible. The observed 2D lattice appears to be quite anisotropic: $b/a \approx 2.42$. This corresponds to a strong deviation from a hexagonal columnar phase for which $b/a = \sqrt{3}$.

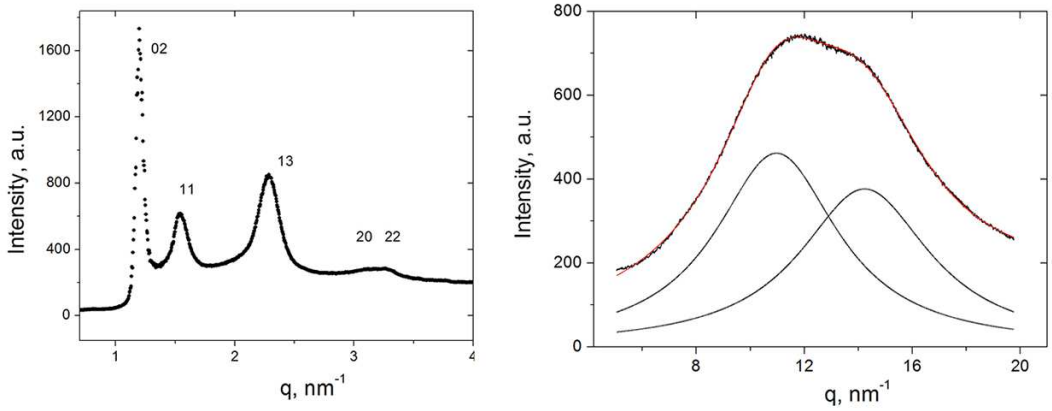

Fig. 4. X-ray diffraction profile of the G-5-homo dendrimer. (a) Small-angle region with peaks indexed as discussed in the text. (b) Diffuse peaks in the wide-angle region. The solid line fitted to the data points is the sum of two Lorentzian peaks shown below.

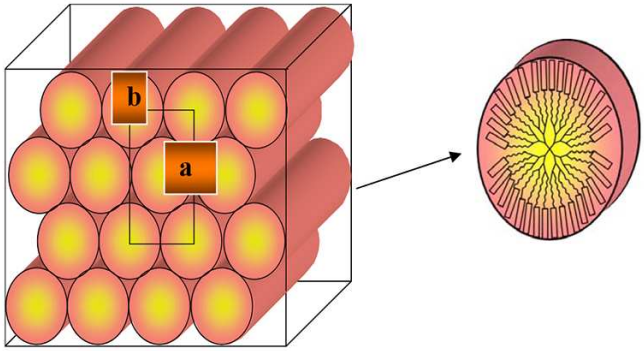

Fig. 5. Left: Schematic view of the columnar rectangular phase ($\mathrm{Col_{rec}}$) formed by the G-5-homo dendrimer with a 2D centered rectangular lattice (parameters a and b). In the third direction (along c) the system displays liquid-like order. Right: Ellipsoidal cross-section (prolate) of an individual dendritic molecule.

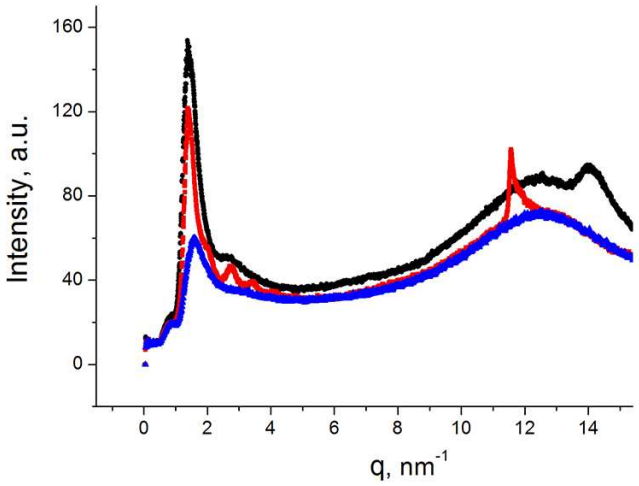

Fig. 6. Radial scans of the 2D scattering pattern combining small- and wide-angle data for the G-2-stat dendrimer. Black curve: $\mathrm{Cr_1}$ phase at $T = -23\,^{\circ}\mathrm{C}$; red curve: $\mathrm{Cr_2}$ phase at $T = -6\,^{\circ}\mathrm{C}$; blue curve: I phase at $T = 4\,^{\circ}\mathrm{C}$.

3.2 G-2-stat dendrimer

For the G-2-stat dendrimer X-ray diffraction shows in the isotropic phase two diffuse peaks in the small- and wide-angle region, respectively (see fig. 6). The first peak is centered at $q \approx 1.57\,\mathrm{nm}^{-1}$ corresponding to a dimension $d \approx 4\,\mathrm{nm}$. The correlation length is of the same order of magnitude, $\xi \approx 4.6\,\mathrm{nm}$. Assuming that the dendrimer spheres are locally closely packed (fcc lattice), their average diameter would tentatively be $D = d\sqrt{3}/\sqrt{2} \approx 4.9\,\mathrm{nm}$. From the position of the wide-angle peak at $q \approx 12.6\,\mathrm{nm}^{-1}$, the average distance between the molten aliphatic (aromatic) and carbosilane moieties within the dendritic spheres can be calculated to be about 0.5 nm.

The transition to the intermediate $\mathrm{Cr_2}$ phase is signaled in the wide-angle region by the appearance of an additional narrow (crystalline) peak centered at $q \approx 11.6\,\mathrm{nm}^{-1}$ ($2\pi/q = 0.54\,\mathrm{nm}$). Finally in the $\mathrm{Cr_1}$ phase (below $-16.5\,^{\circ}\mathrm{C}$) a splitting into two peaks occurs with corresponding lengths of about 0.5 and 0.44 nm. A further analysis of the crystalline order is outside the scope of this paper. Nevertheless we conclude that both crystalline phases possess a considerable amorphous component, indicative either of a highly defective crystalline phase or of coexistence of two phases (micro-segregation), crystalline and lamellar.

3.3 G-2-block dendrimer

Compared to the G-2-homo dendrimer, the G-2-block one is characterized by both a considerable decrease in the temperature range of the SmA mesophase and a decrease of the isotropic transition temperature. This can be attributed to a decrease in the content of terminal mesogenic groups responsible for LC ordering. Although the G-2-block and G-2-stat dendrimers have the same composition, the clearing point of the former is much higher.

X-ray diffraction of the G-2-block dendrimer shows a number of equally spaced layer reflections at a distance

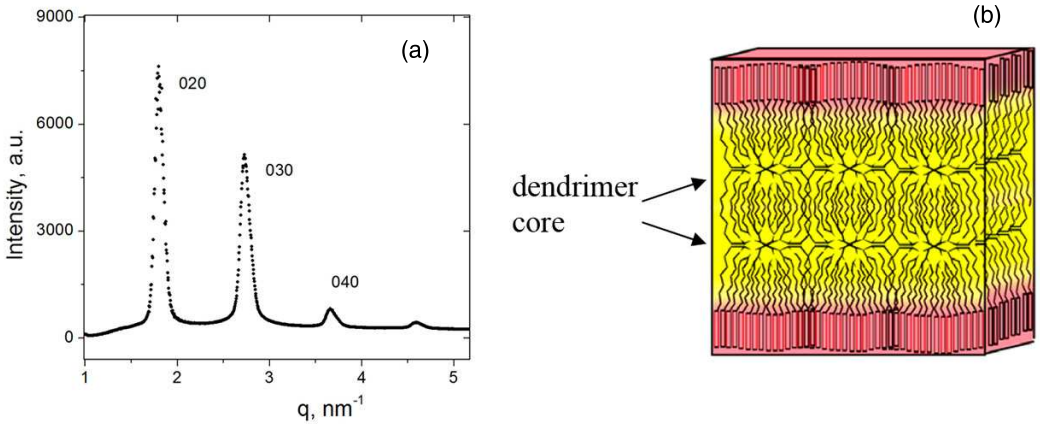

Fig. 7. Structural data of the G-2-block dendrimer. (a) Layer reflections indexed as indicated. (b) Proposed structure of the bilayer smectic A phase.

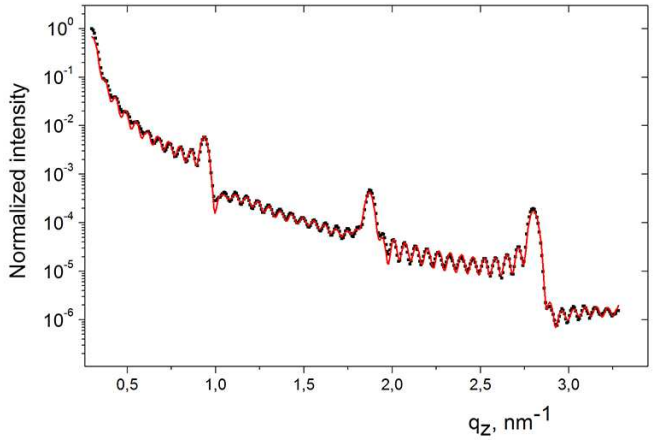

Fig. 8. X-ray reflectivity of a G-2-block dendrimer film. The solid line gives the best fit corresponding to the electron density profile of table 4.

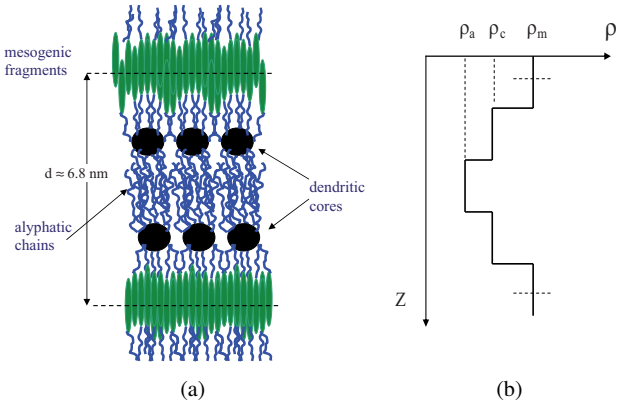

Fig. 9. Model for the smectic layering in G-2-block dendrimer. (a) Cross-section of a single smecic layer with two dendrimer molecules. (b) Schematic representation of the corresponding electron density profile $\rho_e(z)$; ρ_a, ρ_c and ρ_m stand for the density of the aliphatic chains, dendrimer core and mesogenic fragments, respectively.

of 0.926 nm^{-1}, fig. 7a, corresponding to $d \approx 6.78$ nm. The first harmonic is blocked by the beamstop, but its presence has been confirmed in a separate small-angle experiment. The in-plane order is liquid-like with a double peaked diffuse profile, similar as for the homo-dendrimers. To accommodate the observed layer thickness, we need two dendritic molecules per smectic layer, fig. 7b. Avoiding contacts between terminal aromatic and aliphatic chains, we arrive at the scheme of fig. 7b in which azobenzene and aliphatic moieties are segregated with partial overlap of allied fragments. The amount of overlap for given layer thickness is ambiguous and cannot be set *a priori*. Therefore we turned to X-ray reflectivity (XRR) of thin ordered films on a substrate to elucidate the precise nature of the bilayer smectic ordering.

Figure 8 depicts XRR data for one of the block dendrimer films. A transverse scan across the specular reflectivity (not shown) gives a FWHM of typically 0.025°, indicating a well-aligned film. From the oscillations (Kiessig fringes) due to interference of the reflections from each of the two interfaces, we derive a film thickness $L \approx 97.4$ nm. Three orders of Bragg reflections from the smectic layers parallel to the interfaces indicate a periodicity $d \approx 6.73$ nm, close to the bulk value. As starting point for a simulation of the reflected intensity we placed two LC dendrimer molecules in the opposite directions along the layer normal, fig. 9a. The degree of overlap of the segregated aromatic and aliphatic fragments is arbitrary. The model electron density $\rho_e(z)$ is calculated by projecting the different atoms on the z-direction (box or slab model). The molecular fragments are assumed to be in a fully extended configuration, with bond angles and lengths taken from space-filling models. The resulting electron density distribution is schematically shown in fig. 9b. Note that the overlapping aromatic fragments lead to a larger electron density than the dendritic Si matrices, while the aliphatic tails are characterized by the smallest values. The resulting density modulation is obtained by convolution of the box function, fig. 9b, with a Gaussian of width σ, to take layer fluctuations (interface roughness) into account. The values of σ can in principle differ for each interface.

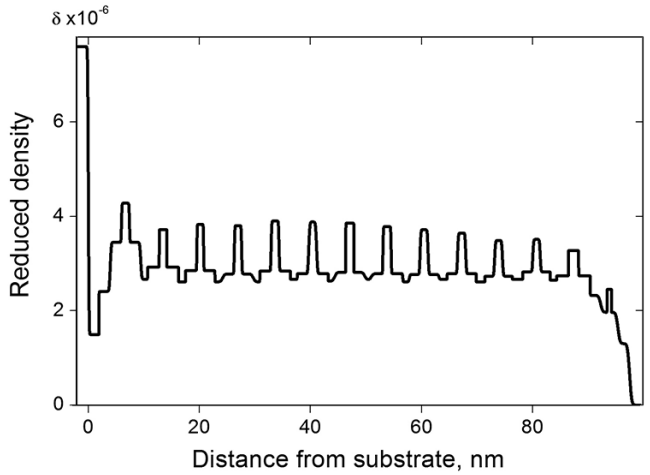

Fig. 10. Model electron density across the G-2-block dendrimer film.

Finally we treated the parameters characterizing each smectic layer as adjustable variables. To do so we constructed a model of 58 independent slabs: a slab at the film-substrate interface, fourteen smectic layers characterized by the four slab box function of fig. 9b, and a slab at the film-air interface. Each slab is characterized by thickness l, interfacial roughness σ and electron density δ (expressed in the dimensionless units of $\delta = \rho_e r_e \lambda^2/2\pi$, where r_e is the classical electron radius). Figure 8 shows the resulting best fit to the XRR data using the parameters given in table 4. Figure 10 illustrates the resulting density profile, which indicates that the smectic lamellae are best developed in the middle of the film. The optimized model consists of a layer adjacent to the substrate of about 1.9 nm, then a strongly distorted smectic layer of 7.5 nm and enhanced density, 11 smectic layers of 6.70 ± 0.02 nm, and two top layers with a reduced density at the film-air interface. The latter effect is directly visible in AFM, which indicates terraces in the top layer over which XRR averages laterally.

From the data in table 4 we conclude that the slabs of lowest density, $\delta \approx 2.6$, belong to overlapping aliphatic chains with $l \approx 1.2$ nm. The length of this fragment in a fully trans configuration is about 1.3 nm, indicating that the hydrocarbon chains fully overlap. The same is true for the aromatic mesogenic fragments (average size 1.4 nm) at the highest electron density $\delta \approx 3.8 \pm 0.2$. The layer adjacent to the substrate has an unusually low electron density, $\delta \approx 1.5$, indicating weak adhesion of the LC dendrimer to the silicone/glass substrate. This can explain why the first smectic layer, merged with the "porous" layer at the silicon substrate, has an enhanced density.

The above finding correlates with the AFM observations (not shown) that indicate one-layer terraces at the free surface of the film, that slowly (on a scale of weeks) evolve into deeper holes. Finally dewetting occurs, accompanied by the formation of macroscopic droplets and a precursor monomolecular film. Such a behaviour is typical for many polymer and LC films in contact with substrates [48,49].

Table 4. Model parameters for best fit of reflectivity data for the G-2-block dendrimer film. There are nine repetitive sells in the film interior.

Model: 58 independent slabs			
$\delta_{\text{av.}} = 2.88 \cdot 10^{-6}$		Total thickness 97.4 nm	
l (nm)	$\delta \cdot 10^{-6}$	σ (nm)	Description
–	7.60	0.0	Si-substrate
1.92	1.49	0.01	Intermediate slab
2.01	2.41	0.15	Cell of 4 slabs
2.03	3.45	0.07	
1.43	4.28	0.07	
2.03	3.45	0.07	
1.23	2.67	0.01	Cell of 4 slabs
2.10	2.92	0.01	
1.37	3.72	0.01	
2.10	2.92	0.01	
1.29	2.61	0.01	Cell of 4 slabs
2.03	2.85	0.05	
1.21	3.83	0.05	
2.03	2.85	0.01	
...	...	...	...
1.18	2.65	0.01	Cell of 4 slabs
2.10	2.74	0.01	
1.85	3.27	0.01	
2.10	2.74	0.01	
1.85	2.33	0.30	Cell of 4 slabs
1.15	1.97	0.01	
0.80	2.45	0.01	
1.15	1.97	0.30	
2.10	1.30	0.30	Slab at the air interface
Air			

4 Discussion

Several attempts have been made to understand the behaviour of various types of LC dendrimers, both from the point of view of molecular theory [50,51] and using computer simulations [52]. In the latter case a molecular dynamics study with 100 dendrimer molecules indicates for carbosilane LC dendrimer of third generation at relatively high density lamellar ordering with fully overlapping terminal mesogenic units. Molecular theory is still challenging due to complexity of the problem. LC dendrimers have several topologically and chemically dif-

ferent segments, producing many combinations of intra- and inter-dendrimer segmental interactions [51]. Moreover, the flexibility of the spacers and other constituent fragments is an important factor in determining the stability of the various structures that cannot easily be incorporated.

For the ideal case of complete and perfect connectivity, the branch hierarchy of dendrimer molecule can be represented by series of regular, radially concentric layers around the core, fig. 1. Each of the layers contains a precise number of branching points, the number of which increases exponentially from the core to the exterior. However, there are severe restrictions to the existence of the LC dendrimers of higher generations. First with increasing generation the molecules will experience steric hindrance at their focal points that become "buried" within the developing bulk. This can be described as reduced "reactivity" of the focal points in higher generation dendrimers, may significantly restrict the reproducibility of the growth process and increase the probability of defect formation [53].

Most importantly, dendrimers with terminal groups cannot remain perfect when exceeding a certain size because they eventually become too congested. With increasing n the available surface area is increasingly less sufficient, and at a certain stage no ideal growth is sterically possible anymore [54,55]. This can be understood by counting the number of monomers in each generation. For functionalities of the core, $f_c = 4$, and branching points, $f = 3$, characteristic of carbosilane dendrimers, the number of terminal positions m varies with generation number as $m_n = 2^{n+2}$. Varying n from 0 to 5, this leads to m_n values equal to 4, 8, 16, 32, 64, and 128, respectively. Hence for $n = 5$ more than half the monomers are in the last generation: $m_5/\Sigma m_{0-4} = 128/124 > 1$. As the volume occupied by the terminal groups cannot exceed the accessible volume, this leads for a perfect dendrimer to a maximum generation [56]. To make a higher generation, either monomers with a larger aspect ratio should be used, or, alternatively, short alkyl chains should be introduced between the branching points of the core.

Lezov *et al.* [57] studied in detail the viscous properties of the carbosilane dendrimers with terminal mesogenic groups for $n = 1$–5. The hydrodynamic radius, calculated from the measured viscosity, systematically increases with the dendrimer generation. Defining R_{core} as the core radius of the dendrimer molecule, the surface area per the end-chain, $S_m = 4\pi R^2{}_{\text{core}}/m$, was found to scale with the number of terminal positions as $S_m \sim m^{-0.3}$, in agreement with theoretical calculations that give a value of 1/3 for the exponent [54]. Hence upon increasing n from 1 to 5 the specific surface area S_m diminishes by more than a factor 2. Once the available surface area of the dendrimer is less than the total area required for packing all end-groups together, the terminal chains must stretch and orient themselves perpendicular to the core surface. In practice, carbosilane dendrimers with terminal mesogenic groups are for $n \geq 6$ of limited use due to their incomplete surface coverage.

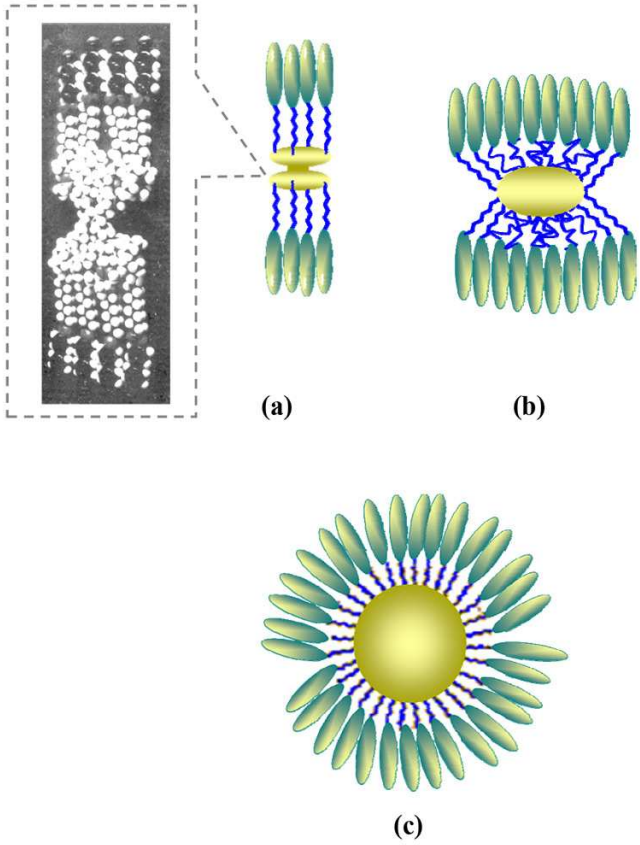

Fig. 11. Cross-sections of the individual dendrimer molecules favoring the formation of the lamellar (a, b) and columnar (c) phases. The inset at (a) shows the Stuart-Briegleb molecular model for the first generation LC dendrimer. The cylindrical-like conformation of the first (a) and the third (b) generations favors smectic layering. For the fifth generation (c) the terminal chains are stretched and orient preferably perpendicular to the core surface.

From the discussion so far the following picture emerges. For generations $n \leq 4$, the molecules may be accommodated in a lamellar structure because they can adopt roughly a cylindrical shape and fit into a layer (see in fig. 11a, b). This is only possible for low generations, for which the density of terminal fragments at the periphery is low enough to afford a planar configuration and interdigitation of mesogenic fragments from neighboring layers. This picture applies to both homo and block dendrimers. However, for $n = 5$ the mesogenic chains are forced to orient preferably perpendicular to the core surface, fig. 11c. As a result the molecules become more elliptical, and the terminal chains cannot penetrate into each other anymore (shown schematically in fig. 12). This drives the formation of a columnar phase rather than continuous layers (bilayers). In this situation the free energy of the system increases due to loss of entropy related to a more ordered state. However, this is compensated by a decrease in energy associated with the distortion of the cylindrical conformation characteristic of the lamellar phase, fig. 11. Though this picture reflects the general

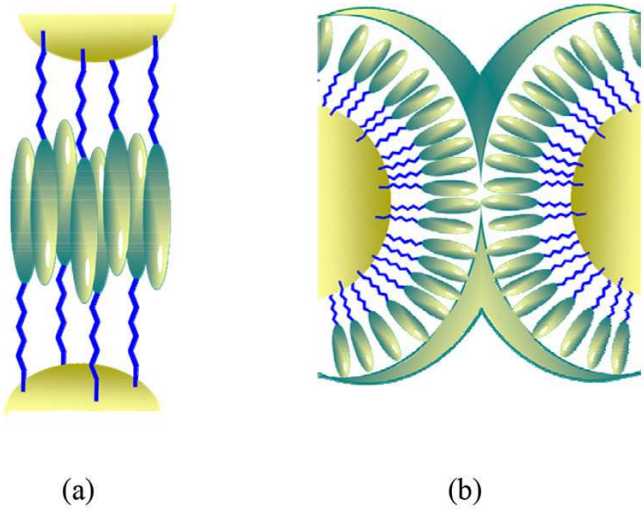

Fig. 12. Models of interacting LC dendrimers for (a) $n \leq 4$, and (b) $n = 5$.

trend in the phase behavior of LC dendrimer molecules, examples of LC carbosilane dendrimers exist with a more complicated phase behavior [22,37]. Upon cooling from the isotropic phase a sequence columnar-lamellar smectic-crystalline may occur.

The G-2-block dendrimer forms bilayer smectic ordering with an antiparallel arrangement of two dendritic molecules. Evidently this is due to the incompatibility between the aromatic and aliphatic parts, similar to the microphase separation in diblock and triblock copolymers [58] or diluted side-chain mesogenic polymers [59]. The LC block-dendrimer can be considered as part of a broader class of polyphilic LC materials, in which building blocks with different types of interaction sites are combined (for example, aliphatic, aromatic, fluoro, and siloxane-based fragments) [14–16]. In addition to low-molecular-mass polyphilic molecules [60], such systems include hybrid LC block copolymers [61], rod-coil molecules [62] and cyclic siloxane oligomers [63,64].

In the G-2-stat dendrimer the incompatible aliphatic and aromatic fragments are randomly tethered at the core periphery. Hence microphase segregation as in block-dendrimers is not possible and no mesogenic phase is observed. Instead two crystalline phases of diverse symmetry have been observed with a direct transition to the isotropic phase. Evidently, at the surface of the dendritic matrix there is a crucial decrease in the amount of pair contacts of terminal mesogenic groups responsible for LC ordering.

Finally, the in-plane structure factor in both smectic and columnar phases of the LC dendrimers reveals a splitting of the intensity profiles into two diffuse peaks (characteristic spacings $d_1 \approx 0.57\,\text{nm}$ and $d_2 \approx 0.44\,\text{nm}$). Evidently, certain molecular fragments pack less tightly than others. Such behaviour has been observed in several complex molecular systems [65]. Examples are discotic mesophases [66], containing flexible, almost molten hydrocarbon tails, and polymer LCs [67] in which mesogenic moieties behave almost independently of the main chains. Other examples are polyphilic mesogens consisting of aromatic, aliphatic and fluorinated fragments [14, 15] and monolayers of semifluorinated alkanes [68]. In our situation, for hexagonal local packing, the in-plane periodicities correspond to average nearest-neighbor molecular separations, $a = 2d/\sqrt{3}$, of about 0.66 and 0.51 nm. The latter distance is clearly related to the densely packed disordered hydrocarbon chains of average diameter $a \approx 0.49\,\text{nm}$ [14,15]. Rotationally averaged aromatic fragments give similar values around $a \approx 0.52\,\text{nm}$. However, the mean distance associated with local packing of disordered oligosiloxane or carbosilane chains is around 0.6–0.8 nm [69,70]. Thus we tentatively attribute the larger of the observed separations, $a \approx 0.66\,\text{nm}$, to short-range correlations of mutually disordered carbosilane fragments within the dendrimer matrix.

5 Conclusions

We have studied homo-, block-, and statistical dendrimers with different surface topology of mesogenic groups and aliphatic decyl chains. The homo-dendrimers of low generation can adopt a roughly cylindrical shape that fits into a lamellar structure. This results in a monolayer smectic phase in which the terminal mesogenic groups from neighboring layers completely overlap. With increasing generation number the surface area available for the mesogenic chains is reduced, the terminal chains become stretched and are forced to orient preferably perpendicular to the core surface. For generation 5 this leads to change in the main molecular conformation: the molecules become elliptical which drives a transition to a columnar phase.

The block-dendrimer of second generation forms bilayer smectic ordering. The chemically distinct aromatic and aliphatic moieties are segregated with complete overlap of the allied fragments. The statistical dendrimer does not show any mesogenic phase. Microphase separation in LC block-dendrimers opens up the opportunity to self-assemble into well-defined nanostructures with potential applications in molecular electronics and photonics. For the present materials, the presence of photo-sensitive azobenzene fragments in one of the terminal chains is especially interesting. Prepared as thin ordered films this opens possibilities for reversible recording and long-term storage of information.

We thank A.I. Lysachkov for his contribution to the synthesis of the LC dendrimers and the study of their phase behaviour and photochromic properties, V.V. Volkov for checking the small angle scattering area for some dendrimer materials and fruitful discussions, R.M. Richardson for providing us with X-ray data on the G-1-homo dendrimer and useful discussions, and P.V. Dorovatovskii for his assistance at beamline "Belok" in Kurchatov Synchrotron Centre, Moscow. The work at Kurchatov Synchrotron Centre was carried out in the framework of the government contract N 16.552.11.7003. Finally we acknowledge stimulating discussions with M. Warner and E.M. Terentjev.

References

1. P. Barois, J. Pommier, J. Prost *Solitons in Liquid Crystals*, edited by L. Lam, J. Prost (Springer, Berlin, 1992) Chapt. 6.
2. R. Blinc, A.P. Levanyuk (Editors), *Incommensurate phases in dielectrics* (Elsevier, 1986).
3. R.J. Birgeneau, P.M. Horn, Science **232**, 329 (1986).
4. P.E. Cladis, Phys. Rev. Lett. **35**, 48 (1975).
5. F. Hardouin, N.H. Tinh, M.F. Achard, A.M. Levelut, J. Phys. Lett. **43**, 327 (1982).
6. L. Longa, W.H. de Jeu, Phys. Rev. A **28**, 2380 (1983).
7. J.O. Indekeu, A.N. Berker, Phys. Rev. A **33**, 1158 (1986).
8. W. Helfrich, J. Phys. **48**, 291 (1987).
9. E. Fontes, P.A. Heiney, J.L. Haseltine, A.B. Smith, J. Phys. **47**, 1553 (1986).
10. T.A. Lobko, B.I. Ostrovskii, W. Haase, J. Phys. II **2**, 1195 (1992).
11. G. Pelzl, I. Latif, S. Diele, M. Novak, D. Demus, H. Sackmann, Mol. Cryst. Liq. Cryst. **139**, 353 (1986).
12. G. Sigaud, F. Hardouin, M. Mauzac, N.H. Tinh, Phys. Rev. A **33**, 789 (1986).
13. J. Watanabe, Y. Nakata, K. Simizu, J. Phys. II **4**, 581 (1994).
14. L.M. Blinov, T.A. Lobko, B.I. Ostrovskii, S.N. Sulianov, F.G. Tournilhac, J. Phys. II **5**, 979 (1995).
15. B.I. Ostrovskii, in *Structure and Bonding, Liquid Crystals I*, edited by D.M.P. Mingos, Vol. **94** (Springer, Berlin, 1999) p. 199.
16. C. Tschierske, J. Mater. Chem. **11**, 2647 (2001).
17. A.W. Bosman, H.M. Janssen, E.M. Meijer, Chem. Rev. **99**, 1665 (1999).
18. B. Donnio, D. Guillon, Adv. Polym. Sci. **201**, 45 (2006).
19. D. Astruc, E. Boisselier, C. Ornelas, Chem. Rev. **110**, 1857 (2010).
20. S.A. Ponomarenko, E.A. Rebrov, N.I. Boiko, N.V. Vasilenko, A.M. Muzafarov, Ya.S. Freidzon, V.P. Shibaev, Polym. Sci. A **36**, 896 (1994).
21. V. Percec, P.W. Chu, G. Ungar, J.P. Zhou, J. Am. Chem. Soc. **117**, 11441 (1995).
22. S.A. Ponomarenko, N.I. Boiko, V.P. Shibaev, Polym. Sci. C **43**, 1 (2001).
23. J. Barbera, B. Donnio, R. Gimenez *et al.*, J. Mater. Chem. **11**, 2808 (2001).
24. H. Hahn, Ch. Keith, H. Lang, R.A. Reddy, C. Tschierske, Adv. Mater. **18**, 2629 (2006).
25. I.M. Saez, J.W. Goodby, Chem. Eur. J. **9**, 4869 (2003).
26. I.M. Saez, J.W. Goodby, in *Structure and Bonding, Liquid Crystalline Functional Assemblies and Their Supramolecular Structures*, edited by D.M.P. Mingos, Takashi Kato, Vol. **128** (Springer, Berlin, 2008) p. 1.
27. J-W. Choi, B-K Cho, Soft Matter **7**, 4045 (2011).
28. N. Gimeno, J. Vergara, M. Cano, J.L. Serrano, M.B. Ros, J. Ortega, C.L. Folcia, S. Rodríguez-Conde, G. Sanz-Enguita, J. Etxebarria, Chem. Mater. **25**, 286 (2013).
29. P.R. Dvornic, M.J. Owen (Editors), *Silicon-Containing Dendritic Polymers, Advances in Silicon Science*, Vol. **2** (Springer Science + Business Media B.V., 2009).
30. V. Shibaev, N. Boiko, ibid, Ch.10 and references therein.
31. S.A. Ponomarenko, E.A. Rebrov, A.Y. Bobrovsky, N.I. Boiko, A.M. Muzafarov, V.P. Shibaev, Liq. Cryst **21**, 1 (1996).
32. K. Lorenz, H. Frey, B. Stuhn, R. Mulhaupt, Macromolecules **30**, 6860 (1997).
33. D. Terunuma, T. Kato, R. Nishio, K. Matsuoka, H. Kuzuhara, Y. Aoki, H. Nohira, Chem. Lett. **27**, 59 (1998).
34. S.A. Ponomarenko, N.I. Boiko, V.P. Shibaev, R.M. Richardson, I.J. Whitehouse, E.A. Rebrov, A.M. Muzafarov, Macromolecules **33**, 5549 (2000).
35. S.A. Ponomarenko, N.I. Boiko, X.M. Zhu, E.V. Agina, V.P. Shibaev, S.N. Magonov, Polym. Sci., Ser. A **43**, 245 (2001).
36. X.M. Zhu, N.I. Boiko, E.A. Rebrov, A.M. Muzafarov, M.V. Kozlovsky, R.M. Richardson, V.P. Shibaev, Liq. Cryst. **28**, 1259 (2001).
37. E.V. Agina, N.I. Boiko, R.M. Richardson, B.I. Ostrovskii, V.P. Shibaev, E.A. Rebrov, A.M. Muzafarov, Polym. Sci. Ser. A **49**, 412 (2007).
38. R.M. Richardson, E.V. Agina, N.I. Boiko, V.P. Shibaev, I. Grillo, J. Phys. Chem. B **112**, 16346 (2008).
39. A.M. Muzafarov, O.B. Gorbatsevich, E.A. Rebrov, G.M. Ignatreva, T.B. Chenskaya, V.D. Myakushev, A.F. Bulkin, V.S. Papkov, Polym. Sci. Ser. A **35**, 1215 (1993).
40. A.I. Lysachkov, N.I. Boiko, E.A. Rebrov, A.M. Muzafarov, V.P. Shibaev, Russ. Chem. Bull., Int. Ed. **56**, 2407 (2007).
41. D.M. Kheiker, M.V. Kovalchuk, Yu.N. Shilin, V.A. Shishkov, S.N. Sulyanov, P.V. Dorovatovskii, A.A. Rusakov, Cryst. Rep. **52**, 358 (2007).
42. S.N. Sulyanov, A.N. Popov, D.M. Kheiker, J. Appl. Cryst. **27**, 934 (1994).
43. S. Sulyanov, H. Boysen, C. Paulmann, E. Sulyanova, A. Rusakov, Z. Kristallogr, Proc. **1**, 175 (2011).
44. L.G. Parrat, Phys. Rev. **95**, 359 (1954).
45. S.B. Astaf'ev, S.F. Borisova, B.M. Shchedrin, L.G. Yanusova, Cryst. Rep. **51**, 685 (2006).
46. S.B. Astaf'ev, B.M. Shchedrin, L.G. Yanusova, Crystallografia **57**, 141 (2012) (in Russian).
47. *International Tables for Crystallography*, Volume A, fifth edition (Kluwer Acad. Publ., Dordrecht, Boston, London, 2002), page 91.
48. G. Reiter, A. Sharma, R. Khanna, A. Casoli, M.-O. David, J. Colloid Interface Sci **214**, 126 (1999).
49. A Sharma, Eur. Phys. J. E **12**, 397 (2003) and references therein.
50. A.F. Terzis, A.G. Vanakaras, D.J. Photinos, Mol. Cryst. Liq. Cryst. **330**, 517 (1999).
51. A.G. Vanakaras, D.J. Photinos, J. Mater. Chem. **15**, 2002 (2005).
52. Z.E. Hughes, M.R. Wilson, L.M. Stimson, Soft Matter **1**, 436 (2005).
53. P.R. Dvornic, M.J. Owen in P.R. Dvornic, M.J. Owen (Editors), *Silicon-Containing Dendritic Polymers*, *Advances in Silicon Science*, Vol. **2** (Springer Science + Business Media B.V. 2009) chapt. 1, and references therein.
54. P.G. de Gennes, H. Hervet, J. Phys. (Paris) Lett. **44**, L351 (1983).
55. M. Warner, J. Chem. Soc. Faraday Trans. **87**, 861 (1991).
56. M. Rubinstein, R.H. Colby, *Polymer Physics* (Oxford University Press, 2003), p. 308.
57. A.V. Lezov, A.B. Mel'nikov, G.E. Polushina, E.A. Antonov, M.E. Novitskaya, N.I. Boiko, S.A. Ponomarenko, E.A. Rebrov, V.P. Shibaev, E.I. Ryumtsev, A.M. Muzafarov, Dokl. Chem. **381**, 313 (2001).
58. See, for example, F.S. Bates, G.H. Fredrickson, Annu. Rev. Phys. Chem. **41**, 525 (1990), and references therein.

59. S. Diele, S. Oelsner, F. Kuschel, B. Hisgen, H. Ringsdorf, Mol. Cryst. Liq. Cryst. **155**, 393 (1988).
60. F. Tournilhac, L. Bosio, G.F. Nicoid, J. Simon, Chem. Phys. Lett. **145**, 452 (1988).
61. G.C.L. Wong, J. Commandeur, H. Fischer, W.H. de Jeu, Phys. Rev. Lett. **77**, 5221 (1996).
62. M. Lee, B.K. Cho, K.J. Ihn, W.K. Lee, N.K. Oh, W.C. Zin, J. Am. Chem. Soc. **123**, 4647 (2001).
63. H. Wang, M.Y. Jin, R.C. Jarnagin, T.J. Bunning, W. Adams, B. Cull, Y. Shi, S. Kumar, E.T. Samulski, Nature **384**, 244 (1996).
64. P.I.C. Teixeira, E.M. Terentjev, Europhys. Lett. **46**, 364 (1999).
65. S. Shin, N. Collazo, S.A. Rice, J. Chem. Phys. **96**, 1352 (1992).
66. E. Fontes, P.A. Heiney, M. Ohba, J.N. Haseltine, A.B. Smith, Phys. Rev. A **37**, 1329 (1988).
67. P. Davidson, P. Keller, A.M. Levelut, J. Phys. (Paris) **46**, 939 (1985).
68. A. Mourran, B. Tartsch, M. Gallyamov, S. Magonov, D. Lambreva, B.I. Ostrovskii, I.P. Dolbnya, W.H. de Jeu, M. Moeller, Langmuir **21**, 2308 (2005).
69. Ch. Keith, R.A. Reddy, A. Hauser, U. Baumeister, C. Tschierske, J. Am. Chem. Soc. **128**, 3051 (2006).
70. R. Kieffer, M. Prehm, K. Pelz, U. Baumeister, F. Liu, H. Hahn, H. Lang, G. Ungar, C. Tschierske, Soft Matter **5**, 1214 (2009).